Ultra high bandwidth WDM using silicon microring modulators

Sasikanth Manipatruni[1*], Long Chen[1] and Michal Lipson[1,2]

[1]*School of Electrical and Computer Engineering, Cornell University, Ithaca, NY 14853, USA*
[2]*Kavli Institute at Cornell for Nanoscale Science, Ithaca, NY 14853, USA*
**sm448@cornell.edu*

Abstract: We report 50 Gbit/s modulation capability using four silicon micro ring modulators within a footprint of 500 μm^2. This is the highest total modulation capability shown in silicon using compact micro-ring modulators. Using the proposed techniques, silicon nanophotonic bandwidths can meet the requirements of future CMOS interconnects by using multiple wavelengths to extend beyond single device speeds.

OCIS codes: (250.3140) Integrated optoelectronic circuits; (250.6715) Switching; (230.4555) Coupled resonators; (230.3120) Integrated optics devices.

References and links

1. I. A. Young, E. Mohammed, J. T. S. Liao, A. M. Kern, S. Palermo, B. A. Block, M. R. Reshotko, and P. L. D. Chang, "Optical I/O Technology for Tera-Scale Computing," IEEE J. Solid-state Circuits **45**(1), 235–248 (2010).
2. D. A. B. Miller, "Device Requirements for Optical Interconnects to Silicon Chips," Proc. IEEE **97**, 1166–1185 (2009).
3. A. V. Krishnamoorthy, *et al*., "The integration of silicon photonics and VLSI electronics for computing systems intra-connect," Proc. SPIE **7220**, 72200V (2009).
4. C. Batten, *et al*., "Building Manycore Processor-to-DRAM Networks with Monolithic Silicon Photonics," High-Performance Interconnects, Symposium on, pp. 21–30, 16th IEEE Symposium on High Performance Interconnects, 2008.
5. R. Beausoleil, et al, "A Nanophotonic Interconnect for High-Performance Many-Core Computation," in Integrated Photonics and Nanophotonics Research and Applications, (Optical Society of America, 2008), paper ITuD2.
6. A. Shacham, K. Bergman, and L. P. Carloni, *On the Design of a Photonic Network-on-Chip*, Networks-on-Chip (2007), pp. 53–64.
7. N. Kirman, *et al*., "Leveraging Optical Technology in Future Bus-based Chip Multiprocessors," Microarchitecture, 2006. MICRO-39. 39th Annual IEEE/ACM International Symposium on, vol., no., pp.492–503, 9–13 Dec. 2006.
8. International Technology Roadmap for Semiconductors, (ITRS 2007).
9. A. Liu, R. Jones, L. Liao, D. Samara-Rubio, D. Rubin, O. Cohen, R. Nicolaescu, and M. Paniccia, "A high-speed silicon optical modulator based on a metal-oxide-semiconductor capacitor," Nature **427**(6975), 615–618 (2004).
10. S. Manipatruni, Q. Xu, B. Schmidt, J. Shakya, and M. Lipson, "High Speed Carrier Injection 18 Gb/s Silicon Micro-ring Electro-optic Modulator," LEOS 2007, IEEE LEOS 2007 Annu. Meeting, Paper WO2, 537–538 (2007).
11. L. Zhou, and A. W. Poon, "Silicon electro-optic modulators using p-i-n diodes embedded 10-micron-diameter microdisk resonators," Opt. Express **14**(15), 6851–6857 (2006).
12. B. Schmidt, Q. Xu, J. Shakya, S. Manipatruni, and M. Lipson, "Compact electro-optic modulator on silicon-on-insulator substrates using cavities with ultra-small modal volumes," Opt. Express **15**(6), 3140–3148 (2007).
13. W. M. Green, M. J. Rooks, L. Sekaric, and Y. A. Vlasov, "Ultra-compact, low RF power, 10 Gb/s silicon Mach-Zehnder modulator," Opt. Express **15**(25), 17106–17113 (2007).
14. G. Gunn, "CMOS photonicsTM - SOI learns a new trick," in Proceedings of IEEE International SOI Conference Institute of Electrical and Electronics Engineers, New York, (2005), 7–13.
15. A. Liu, L. Liao, D. Rubin, H. Nguyen, B. Ciftcioglu, Y. Chetrit, N. Izhaky, and M. Paniccia, "High-speed optical modulation based on carrier depletion in a silicon waveguide," Opt. Express **15**(2), 660–668 (2007).
16. M. R. Watts, D. C. Trotter, R. W. Young, and A. L. Lentine, "Ultralow power silicon microdisk modulators and switches," *Group IV Photonics, 2008 5th IEEE International Conference on*, vol., no., pp.4–6, 17–19 Sept. 2008.
17. X. Zheng, J. Lexau, Y. Luo, H. Thacker, T. Pinguet, A. Mekis, G. Li, J. Shi, P. Amberg, N. Pinckney, K. Raj, R. Ho, J. E. Cunningham, and A. V. Krishnamoorthy, "Ultra-low-energy all-CMOS modulator integrated with driver," Opt. Express **18**(3), 3059–3070 (2010).
18. J. Zhang, T. Y. Liow, G. Q. Lo, and D. L. Kwong, "10Gbps monolithic silicon FTTH transceiver without laser diode for a new PON configuration," Opt. Express **18**(5), 5135–5141 (2010).
19. Silicon carrier dispersion modulators are ultimately limited by the carrier saturation velocity, due to free carrier–optical phonon interactions. In silicon, optical phonons limit the maximum speed of carriers to 10 ps per micron

#129915 - $15.00 USD Received 11 Jun 2010; revised 13 Jul 2010; accepted 13 Jul 2010; published 23 Jul 2010

of transit length, which limits the maximum bandwidth to ~100 Gbit/s for a typical transverse carrier transit distance of 1 micron.
20. S. Manipatruni, Q. Xu, and M. Lipson, "PINIP based high-speed high-extinction ratio micron-size silicon electrooptic modulator," Opt. Express **15**(20), 13035–13042 (2007).
21. F. Caignet, S. Delmas-Bendhia, and E. Sicard, "The challenge of signal integrity in deep-submicrometer CMOS technology," Proc. IEEE **89**(4), 556–573 (2001).
22. M. A. Popovic, E. P. Ippen, and F. X. Kartner, "Low-Loss Bloch Waves in Open Structures and Highly Compact, Efficient Si Waveguide-Crossing Arrays," *Lasers and Electro-Optics Society, 2007. LEOS 2007. The 20th Annual Meeting of the IEEE*, vol., no., pp.56–57, 21–25 Oct. 2007.
23. S. G. Johnson, C. Manolatou, S. Fan, P. R. Villeneuve, J. D. Joannopoulos, and H. A. Haus, "Elimination of cross talk in waveguide intersections," Opt. Lett. **23**(23), 1855–1857 (1998).
24. Q. Xu, B. Schmidt, J. Shakya, and M. Lipson, "Cascaded silicon micro-ring modulators for WDM optical interconnection," Opt. Express **14**(20), 9431–9435 (2006).
25. S. Manipaturni, K. Preston, L. Chen, and M. Lipson, "Ultra-Low Voltage, Ultra Small Mode Volume Silicon Nanophotonic Modulator. Submitted.
26. P. Dong, S. F. Preble, and M. Lipson, "All-optical compact silicon comb switch," Opt. Express **15**(15), 9600–9605 (2007).
27. F. Xia, L. Sekaric, and Yu. A. Vlasov, "Ultra-compact optical buffers on a silicon chip," Nat. Photonics **1**(1), 65–71 (2007).
28. T. Barwicz, M. A. Popovic, P. T. Rakich, M. R. Watts, F. X. Kaertner, E. P. Ippen, and H. I. Smith, "Fabrication Control of the Resonance Frequencies of High-Index-Contrast Microphotonic Cavities," in Integrated Photonics Research and Applications/Nanophotonics, (Optical Society of America, 2006), paper JWA3.
29. SILVACO International, 4701 Patrick Henry Drive, Bldg. 1, Santa Clara, CA 94054.
30. P. D. Hewitt, and G. T. Reed, "Improved modulation performance of a silicon p-i-n device by trench isolation," J. Lightwave Technol. **19**(3), 387–390 (2001) (CrossRef).
31. B. Jalali, O. Boyraz, D. Dimitropoulos, and V. Raghunathan, "Scaling laws of nonlinear silicon nanophotonics," Proc. SPIE **5730**, 41–51 (2005).
32. R. Soref, and B. Bennett, "Electrooptical effects in silicon," IEEE J. Quantum Electron. **23**(1), 123–129 (1987).
33. H. C. Huang, S. Yee, and M. Soma, "Quantum calculations of the change of refractive index due to free carriers in silicon with nonparabolic band structure," J. Appl. Phys. **67**(4), 2033–2039 (1990).
34. S. M. Sze, Physics of Semiconductor Devices. 2nd ed. New York, NY: Wiley, 1981. ISBN: 047109837X.
35. M. Notomi, and S. Mitsugi, "Wavelength conversion via dynamic refractive index tuning of a cavity," Phys. Rev. A **73**(5), 051803 (2006).
36. The chirp associated with this leading edge transient can play a critical role in determining the distance over which the interconnect can be deployed.
37. I. Shake, H. Takara, and S. Kawanishi, "Simple Measurement of Eye Diagram and BER using High-Speed Asynchronous Sampling," J. Lightwave Technol. **22**(5), 1296–1302 (2004).
38. A. Biberman, S. Manipatruni, N. Ophir, K. Bergman, L. Chen, and M. Lipson, "First demonstration of long-haul transmission using silicon microring modulators," submitted to Opt. Express.
39. http://www.picosecond.com/product/product.asp?prod_id=94
40. http://www.shf.de/en/communication/products/rf_broadband_amplifier/40_gbps_rf_amplifier/
41. J. T. Robinson, S. F. Preble, and M. Lipson, "Imaging highly confined modes in sub-micron scale silicon waveguides using Transmission-based Near-field Scanning Optical Microscopy," Opt. Express **14**(22), 10588–10595 (2006).
42. B. Kim, and V. Stojanovic, "Equalized interconnects for onchip networks: Modeling and optimization framework". Int'l Conf. on Computer Aided Design, 2007.
43. A. Liu, L. Liao, Y. Chetrit, J. Basak, H. Nguyen, D. Rubin, and M. Paniccia, "Wavelength Division Multiplexing Based Photonic Integrated Circuits on Silicon-on-Insulator Platform,", " IEEE J. Sel. Top. Quantum Electron. **16**(1), 23–32 (2010).
44. D. W. Kim, A. Barkai, R. Jones, N. Elek, H. Nguyen, and A. Liu, "Silicon-on-insulator eight-channel optical multiplexer based on a cascade of asymmetric Mach-Zehnder interferometers," Opt. Lett. **33**(5), 530–532 (2008).
45. A. C. Turner, C. Manolatou, B. S. Schmidt, M. Lipson, M. A. Foster, J. E. Sharping, and A. L. Gaeta, "Tailored anomalous group-velocity dispersion in silicon channel waveguides," Opt. Express **14**(10), 4357–4362 (2006).
46. S. Manipatruni, R. K. Dokania, B. Schmidt, N. Sherwood-Droz, C. B. Poitras, A. B. Apsel, and M. Lipson, "Wide temperature range operation of micrometer-scale silicon electro-optic modulators," Opt. Lett. **33**(19), 2185–2187 (2008).
47. M. Watts, W. Zortman, D. Trotter, G. Nielson, D. Luck, and R. Young, "Adiabatic resonant microrings (ARMs) with directly integrated thermal microphotonics," In Conference on Lasers and Electro-Optics / Quantum Electronics and Laser Science Conference (CLEO/QELS'09), CPDB10, Baltimore, May 31-June 5 (2009).
48. P. Dong, R. Shafiiha, S. Liao, H. Liang, N.-N. Feng, D. Feng, G. Li, X. Zheng, A. V. Krishnamoorthy, and M. Asghari, "Wavelength-tunable silicon microring modulator," Opt. Express **18**(11), 10941–10946 (2010).

1. Introduction: Scaling the data rates of nanophotonic interconnects

Silicon photonic components are evolving as enablers for highly scalable interconnect solutions for multi-core multi-processors [1–7]. Small foot-print devices are essential for nanophotonic interconnects due to the demand for large bandwidth density (Gbit/s·μm) [8]

#129915 - $15.00 USD Received 11 Jun 2010; revised 13 Jul 2010; accepted 13 Jul 2010; published 23 Jul 2010

and large modulation rate to foot print ratio (Tbit/s.mm^2) [8]. In particular, compact electro-optic modulators can play a critical role in scaling the optical interconnects [1–7]. Hence, it is of great interest to pursue scaling techniques for bandwidths achievable using compact modulators.

Wavelength Division Multiplexing (WDM) is ideally suited for scaling an on-chip optical interconnect due to complexity, foot print and optical insertion loss considerations. Several multi Gbit/s silicon electro-optic modulators have been demonstrated recently, based on a MOS capacitor [9], a PIN diode [10–13] or a PN junction [14–18]. However, the scaling of single wavelength modulation capability is limited fundamentally owing to carrier transport [19], photon lifetime of the optical structures [20], signal integrity limits [21] and high cost of serialization and deserialization. The scaling of interconnect capability using parallel banks of waveguides is limited due to the problem of efficient crossing of multiple waveguides, multiple times with low cross talk and insertion losses [22,23]. Hence, WDM along with a combination of multiplexing schemes are essential to meet the bandwidth requirements of future interconnects.

Here, we extend the modulation capability to 50 Gbit/s using a combination of carrier engineering methods and a wavelength multiplexing scheme. We use four wavelength specific silicon micro-ring based modulators each operating at 12.5 Gbit/s with a total micro-ring device area ~500 μm^2. Prior works in silicon micro-ring modulators have achieved single channel modulation speed of 18 Gbit/s [10] and multi channel modulation capability of 16 Gbit/s (4X4 Gbit/s) [24]. The achieved interconnect density (50 Gbit/s with a 250 nm X 450 nm waveguide, estimated at 33 Gbit/s.μm) is now within the requirements of future high performance computing requirements [8]. To the best of our knowledge, this is the highest modulation capability demonstrated on a single waveguide using micro-ring resonator modulators in a silicon photonic platform [10–14,16–18,24].

2. Wavelength division multiplexing using silicon micro-ring modulators

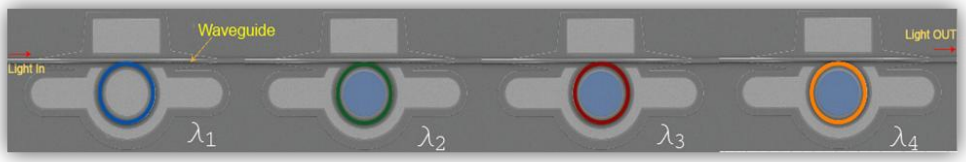

Fig. 1. Microring modulator array (interleaved SEM Image).

We use micro-rings of varying radii to obtain 4 modulators operating at distinct wavelengths (Fig. 1). Travelling wave single mode silicon micro-rings are well suited for WDM due to the wavelength selectivity of the micro-rings [24], scalability to large free spectral range [25], and absence of higher order modes [26]. Each micro-ring modulator is formed by a silicon micro-ring resonator embedded into a PIN diode (Fig. 2). The modulator operates via optical transmission change mediated by free carrier dispersion by injecting and extracting free carriers. The radii of the rings are controlled through fabrication to differ by 20, 40 and 60 nm in circumference (Fig. 3a). The operating wavelengths of the modulators are spread between 1550.0 nm to 1561.2 nm with an inter-channel spacing of 3 ± 1 nm to form a coarse wavelength division multiplexing scheme. The scalability of this scheme depends on the fabrication control of the spacing and repeatability. Earlier works with several micro-rings have shown increasing control over the center wavelengths of micro-ring resonators on silicon-on-insulator substrates [27,28]. We obtained the optical transmission spectrum of the WDM micro-ring bank using a tunable laser with quasi-TE polarized light (Fig. 3b).

#129915 - $15.00 USD Received 11 Jun 2010; revised 13 Jul 2010; accepted 13 Jul 2010; published 23 Jul 2010

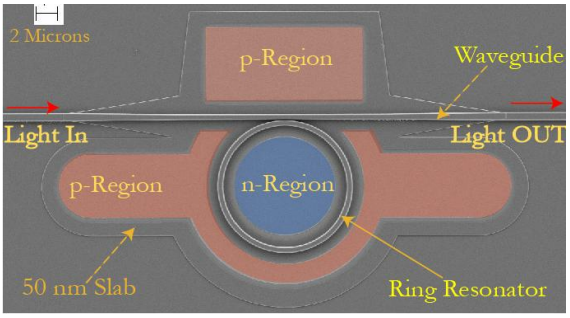

Fig. 2. SEM image of a 6 μm silicon micro-ring modulator created by embedding a micro-ring in a PIN junction. A 50 nm slab is used to electrically contact the waveguide for carrier transport.

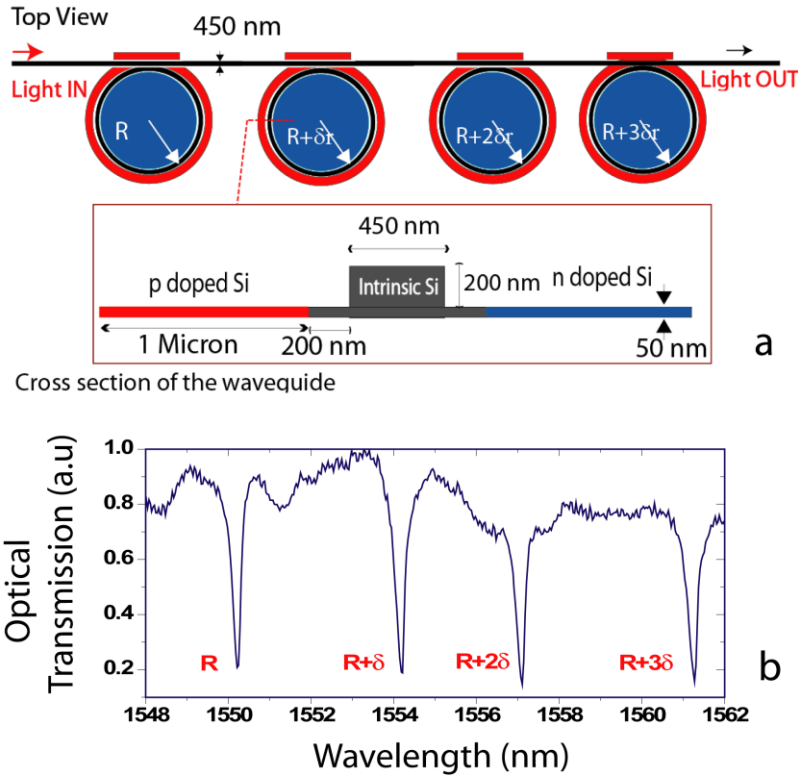

Fig. 3. (a) Schematic of 4 microring modulators coupled to a single waveguide. The inset shows the waveguide cross-section with the doping topology (b) Transmission spectra of 4 microring modulators for quasi-TE polarized light. The radii of the micro-rings are offset by δ = 20 nm.

We fabricated the micro-ring modulators on a silicon on insulator substrate. The top silicon layer (260 nm thick) is used for the passive waveguides and the electro-optical micro-ring modulator. The patterning steps are all performed with electron-beam lithography (JEOL 9300). We defined the silicon waveguides and the ring resonator lithographically and then partially etched the silicon layer to a depth of 210 nm. Another lithography step was used to cover the modulator region and continue the silicon etch, leaving the 50 nm slab only around the modulator for the PIN diodes. After the etching we deposited 20 nm SiO_2 for silicon passivation. Next, we performed the implantation steps for the p-region (outside the rings, BF_2, dose $3X10^{15}/cm^2$ at 45 keV) and n-region (inside the ring, Phosphorous, dose

#129915 - $15.00 USD Received 11 Jun 2010; revised 13 Jul 2010; accepted 13 Jul 2010; published 23 Jul 2010

$2X10^{15}/cm^2$ at 33 keV) respectively. A relatively low temperature anneal (650°C Rapid Thermal Anneal (RTA) for 120s) was subsequently used to activate the dopants. Nickel Silicide was then used for the electrical contacts to the modulator, with 15 nm evaporated nickel and 50 s RTA at 550°C. We then deposited 1 µm SiO_2 top cladding, and patterned via holes and contact pads connecting to the electrodes of the modulator and detector respectively. The doped regions are separated from the waveguide edge by 200 nm to reduce the optical mode overlap with the doped regions. Metal contacts are formed to the center of the ring as well at several points on the periphery. We also note that it is essential to include the PIN diode over the waveguide coupling region to obtain high speed operation. The 50 nm slab region is confined only to the modulator region to allow for low-loss wave guiding to the device from the chip edges.

3. Modeling the electro-optic performance of a silicon micro-ring electro-optic modulator

The modeling of the modulator performance consists of analyzing the electrical response of the electrical PIN structure and the optical response of the micro-cavity. Among other factors, the key parameters determining the response are the cavity photon lifetime and carrier recombination lifetime in the wave-guiding region of the diode.

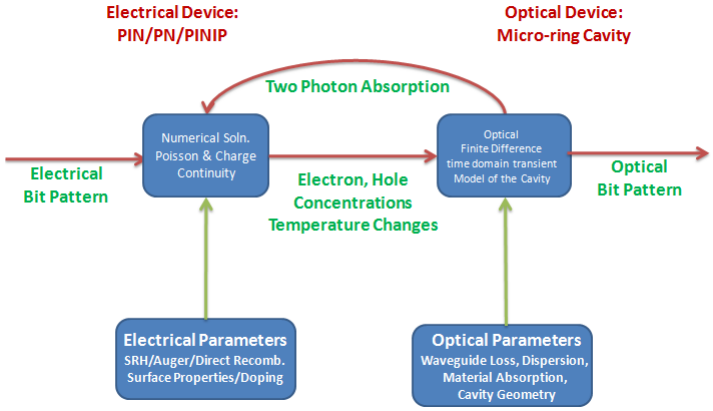

Fig. 4. Schematic of the electro-optic modeling scheme.

Table 1. Electro-optic Simulation Parameters for Silicon Carrier Injection Modulator

Electrical Parameter	Typical Value
Intrinsic region doping	$5x10^{15}/cm^3$
P & N region doping	$10^{20}/cm^3$
Waveguide (width x height)	450 nm x 250 nm
Bulk silicon electron lifetime	3 µs [12]
Bulk silicon hole lifetime	10 µs [12]
Surface recombination velocity	10^4 cm/s [14,16,17]
Interface trap density	10^{10} cm^{-2} eV^{-1} [18]

We modeled the complete transient electro-optic response of the device. The modeling method is shown in Fig. 4. The electrical modeling was carried out in SILVACO device simulation software [29]. The software models the internal physics of the device by numerically solving the Poisson and charge continuity equations. The suitability of SILVACO for simulation of these characteristics has been established by prior works [20,30,31]. We included Shockley Read Hall (SRH), Auger and direct recombination models.

The transient optical response of the device is calculated by finite time difference iterative solution of the micro-cavity optical field. The free carrier dispersion of silicon is modeled using the following equations for the refractive index and absorption coefficient for a

#129915 - $15.00 USD Received 11 Jun 2010; revised 13 Jul 2010; accepted 13 Jul 2010; published 23 Jul 2010

wavelength of 1.55 μm in silicon [32], with a deviation from the classical Drude model [33] due to the non-parabolic band shape

$$\Delta n = \Delta n_e + \Delta n_h = -(8.8\times10^{-22}\,\Delta n + 8.5\times10^{-18}\,\Delta p^{0.8})$$
$$\Delta \alpha = \Delta \alpha_e + \Delta \alpha_h = 8.5\times10^{-18}\,\Delta n + 6.0\times10^{-18}\,\Delta p \qquad (1)$$

where Δn is the change in refractive index, Δα is the change in absorption coefficient of intensity, Δn is the injected electron density per cm^3, and Δp is the injected hole density per cm^3. We outline the models and parameters used in Table 1.

4. Optimizing the speed of a silicon micro-ring electro-optic modulator

The high speed operation of the carrier-injection modulator is enabled by engineering the carrier dynamics to achieve optimal charge injection into the device. The limitation imposed by carrier dynamics over the operation of carrier injection modulators is due to the coupling of the rise and fall time transients. A large turn-on voltage is necessary to enable fast OFF-State to ON-State optical transitions. However, large ON-state voltage leads to excessive injection of the free-carriers. As the electro-optic turn ON voltage is increased to obtain faster turn-ON, the time taken to extract the free carriers increases. This is due to mobility degradation [34] as well as the requirement to extract the excessive charge, leading to limited speed [24].

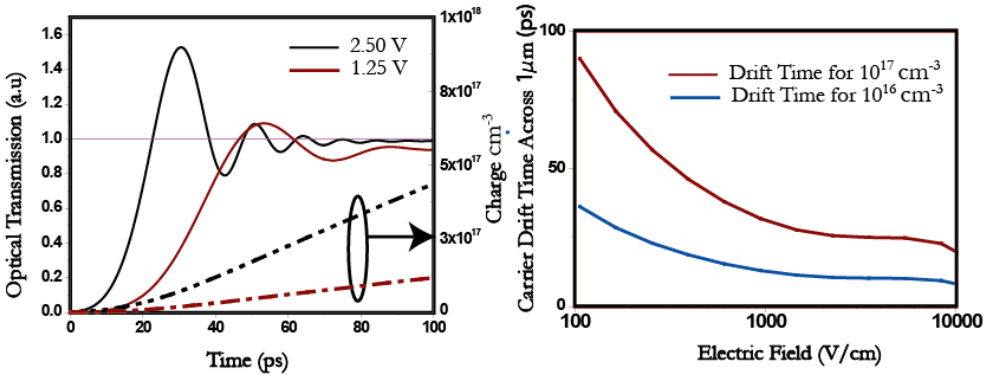

Fig. 5. (a) The transient optical response is shown by the solid line. The transient at the leading edge is due to the interference between light leaking from the cavity with the light coupled straight through the cavity. Dotted lines show the injected charge density for the applied voltages. (b) Time for carriers to drift across 1 micron distance from the center of the waveguide to the doped regions.

The rise and fall times of the carrier injection electro-optic modulator are coupled due to the carrier dynamics. The electro-optic response of the micro-ring modulator to a 1 ns voltage pulse of amplitude 1.25 V is shown in Fig. 5. We see injected carrier density of 1.5 $X10^{17}/cm^3$ for electrons and holes at 100 ps. The optical transient at the leading edge can be attributed to the interference between the stored light leaking from the cavity and the incoming light. The stored light is frequency shifted due to the adiabatic wavelength conversion process in the optical cavity [35,36]. At an applied voltage of 1.25 V, one can see that the optical turn-on can be achieved at 50 ps from the beginning of the transients. To achieve, a 25 ps turn-on time, we can increase the applied voltage to 2.5 V (Fig. 5(a)). However, this significantly affects the turn-off transients, limiting the maximum operation speed of the modulator. In Fig. 5b, we show the time taken for carrier extraction via free carrier drift across the device cross section. As the electro-optic turn ON voltage is increased to obtain faster turn-ON, time taken to extract the free carriers increases (due to mobility degradation [34]) leading to limited speed [26]. We overcome this problem by decoupling the rise and fall time transients.

#129915 - $15.00 USD Received 11 Jun 2010; revised 13 Jul 2010; accepted 13 Jul 2010; published 23 Jul 2010

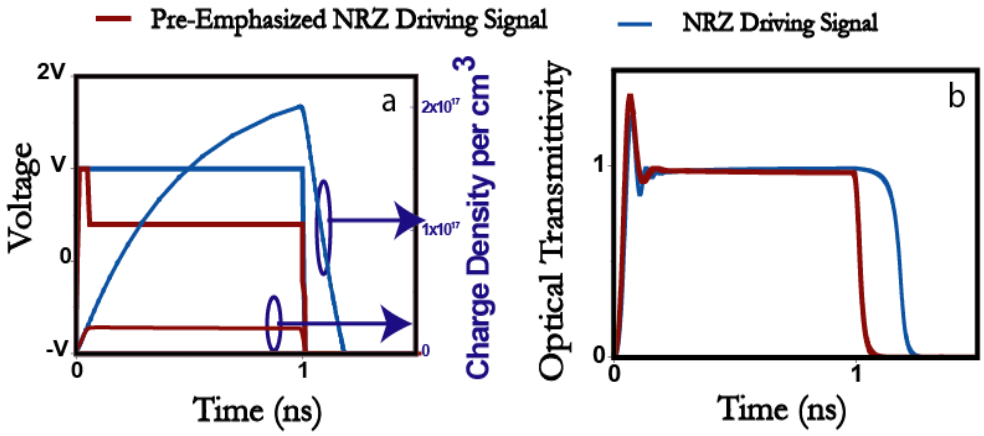

Fig. 6. Driving mechanism for decoupling carrier rise and fall times of an injection modulator. a) applied voltage and charge density response b) The optical response of the modulator. A pre-pulsed signal is applied such that the optical rise time transients are identical while a sharp the fall time transient is achieved during turn-off.

We achieve simultaneous fast turn-ON and fast turn-OFF by controlling the amount of charge injected into the modulator and therefore decoupling the injection and extraction time response. We control the injected charge by engineering the applied voltage into a pre-pulsed Non-Return-Zero pre-pulsed form. The engineered form of the applied voltage is shown in Fig. 6a. A sharp pulse of pulse width equal to or less than a single bit is applied to the pulse with a peak voltage of 2 V. The applied voltage is then reduced to V_{hold} such that the injected current at steady state exactly compensates for free carrier recombination in the waveguide:

$$V_{hold} = V_t + IR + \frac{kT}{e\alpha}\log_e\left(\frac{I}{I_0}+1\right) \qquad (2)$$

where $I = Q/\tau_{recomb}$ is the steady state current through the PIN diode, τ_{recomb} is the carrier recombination lifetime, Q is the total injected charge at steady state, R is the total effective series resistance, k, Boltzmann constant, α the non-ideality coefficient of the diode, I_0 is the reverse saturation current. The Typical parameters for silicon PIN modulators are I_0 ~100 nA, V_t = 0.5 V, α = 0.62, R = 250 Ω. A detailed analytical modeling will be presented elsewhere [25]. The high speed pulse shaping of the applied voltage has previously enabled 18 Gbit/s operation in carrier injection micro-ring modulators [10]. Figure 6 a shows the response of the free carriers to the applied voltages in pre-pulsed and non-pre-pulsed cases. The free carrier response to NRZ signal shows a considerable delay at the falling edge limiting the speed of electro-optic response. One can see that pre-pulsed voltage allows for optimum charge injection while providing a fast carrier extraction transient. The optical response of the modulator is show in Fig. 6b. The optical response of the modulator to the pre-pulsed signal shows both a fast optical turn on and a fast optical turn off enabling ultra fast modulation. This method has previously enabled carrier injection electro-optic modulators to reach 18 Gbit/s [18]. The optical eye diagrams of the modulated signals generated by the modulators are shown in Fig. 8.

5. High speed wavelength division multiplexing using silicon micro-rings

We show high speed Non Return to Zero (NRZ) optical modulation at 4 different wavelengths each at 12.5 Gbit/s. The quality factors of the eye diagrams are estimated as $Q = |\mu_2 - \mu_1|/(\sigma_2 + \sigma_1)$,7.58, 7.36, 8.64, 9.80 all corresponding to very low bit error rates [37,38]. We implemented the driving circuitry with discrete microwave components (Fig. 7). For an analog electronic implementation of a pre-pulsing method on silicon please see [1]. We

#129915 - $15.00 USD Received 11 Jun 2010; revised 13 Jul 2010; accepted 13 Jul 2010; published 23 Jul 2010

generated the pre-pulse signals using an impulse forming network (IFN 5201 [39]) with a transfer function $V_{out} = T_c \, dV_{in}/dt$, where T_c is the derivative time constant. The digital drive signals were pre-amplified using two modulator drivers (JDSU H301) of similar gain and dispersion graphs to amplify the signal in each of the arms. We also used two 20 GHz delay lines to match the signals in time. The signals were then added with a passive 6 dB coupler. Since, the contact resistance of the PIN diodes is only 500 Ω, we have eliminated the final amplifying stage. However, a 20 Gbps amplifier with a large swing voltage (SHF 826 H [40]) can be used if the contact resistance were to be higher. We drove the modulators with 50 Ohm terminated high speed probes. Each modulator is driven by a pre-emphasis method to decouple the injection and extraction times of the device. The DC biases were individually controlled for optimum eye diagrams. A peak to peak driving voltage of 3 V is used to obtain 12.5 Gbit/s operations on each of the four devices.

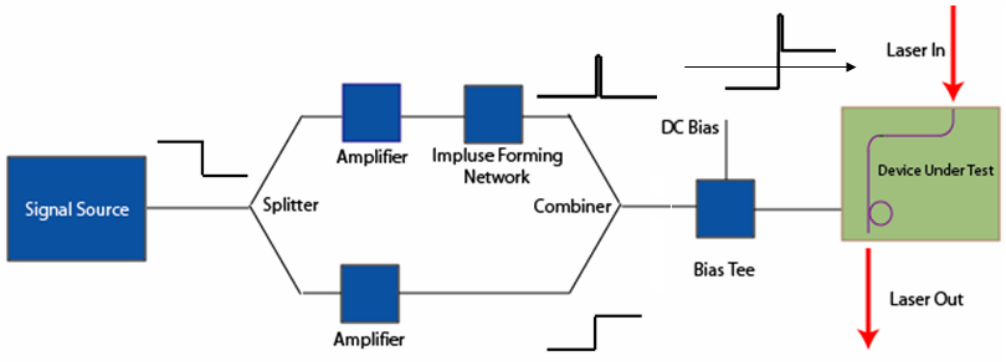

Fig. 7. Driving mechanism for decoupling carrier rise and fall times of an injection. The signal source is divided to generate pre-emphasis signals. The amplifiers are used to control the relative amplitude of the pulses and the data. The pulses are added to the data with appropriate delay.

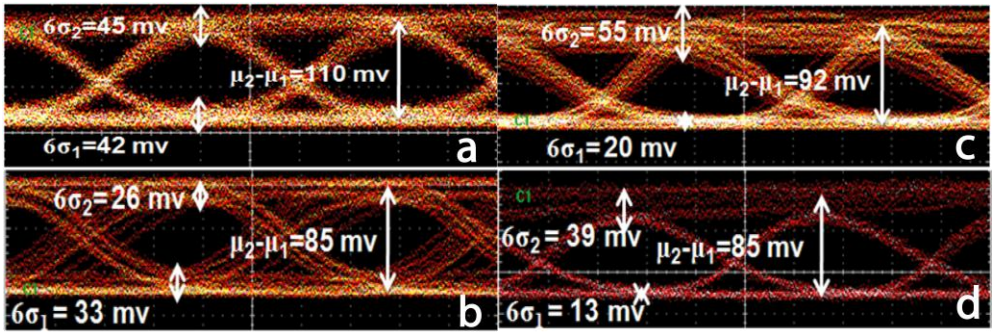

Fig. 8. Optical eye diagrams at 12.5 Gbit/s for 4 micro-ring modulators at a)1562.3 nm b)1558.1 nm c)1555.0 nm d) 1550.7 nm. The variances in the optical high and low state and difference in powers are measured to estimated the quality factor of the eye diagrams. A peak to peak voltage of 3.0 volts was applied.

We show an interconnect bandwidth density for a single waveguide (bandwidth of interconnect/pitch of interconnect) of ~33.3 Gbit/s.μm assuming a center to center waveguide pitch of 1.5 micron. 1.5 micron pitch corresponds to ~20 mm length over which the intensity will suffer a –3dB coupling to the adjacent waveguide assuming two 450 nm X 250 nm waveguides with TE modes. The optical intensity of the TE mode waveguide decays by ~-24 dB compared to the waveguide edge, ($\sim 20\log_{10}(e^{-(pitch-W)/(2t)})$ where W is the waveguide

#129915 - $15.00 USD Received 11 Jun 2010; revised 13 Jul 2010; accepted 13 Jul 2010; published 23 Jul 2010

width, t = $\lambda/15$ is evanescent field transverse decay length [41]. This compares favorably with the bandwidth density requirements for global interconnects for future technology nodes as per ITRS, which predicts 96 nm wide metal interconnects at 2 Gbit/s corresponding to a bandwidth density 20.8 Gbit/s.μm [8]. This is also several times the bandwidth density of optimally repeated global on-chip electrical interconnects today [4,42]. The modulation rate to footprint ratio, a critical figure of merit for optical networks on chip, of this scheme is three orders of magnitude higher than previously demonstrated by using a bank of Mach-Zhender modulators [43,44] while keeping low optical insertion losses. These modulation rate to foot print ratios (~100 Tbit/s·mm^2) can meet the aggressive real estate demands for optical networks for multi-chip multi-processors [4].

6. Design considerations for cascaded micro-ring WDM modulators

The critical design considerations for cascaded micro-ring WDM are a) the channel spacing, and b) the total number of channels set by micro-ring FSR c) Interconnect Bandwidth Density. We note that travelling wave single mode waveguide micro-rings are ideally suited for WDM among the silicon micro-resonators. Micro disc resonators suffer from secondary modes which interfere with WDM operation [11,16].

6.1 WDM microring channel spacing

The spacing between the micro-rings can be controlled accurately by considering the effect of waveguide and material dispersion. The functional dependence of resonance position of the rings can be given by:

$$\omega_k = \frac{r n_{eff}(\omega_0)}{(r+\delta r_k) n_{eff}(\omega_k)} \omega_0 \tag{3}$$

where ω_k is the resonant frequency of the kth micro-ring, $r\omega_0 n_{eff}(\omega_0) = mc$ is valid at the base micro-ring resonance wavelength ω_0, r is the radius of the base micro-ring, δr_k is the radius perturbation introduced in the kth ring. We note that for a WDM microring bank spanning several 10s of nm, a uniform channel spacing ($\delta\omega$) in frequency can be obtained using:

$$\delta r_k = r\left(\frac{\omega_0 n_{eff}(\omega_0)}{(\omega_0 + \delta\omega \cdot k)\cdot n_{eff}(\omega_0 + \delta\omega \cdot k)} - 1\right) \tag{4}$$

where δr_k will be a non-linear spacing variation obtained by considering the strong waveguide dispersion of high index contrast systems [45], waveguide bending, and the material dispersion of the media given by Sellmeier equations. $\delta r_0 = 0$ for the base micro-ring.

6.2 Total number of available WDM channels

The total free spectral range and the number of WDM channels available can be maximized by using minimum sized micro-ring modulators [25]. The free spectral range ($\Delta\omega = \omega_2 - \omega_1$) is given by:

$$\Delta\omega = \left(\frac{c}{r n_{eff}(\omega_2)} - \frac{\Delta n_{eff}}{n_{eff}(\omega_2)}\omega_2\right) \tag{5}$$

#129915 - $15.00 USD Received 11 Jun 2010; revised 13 Jul 2010; accepted 13 Jul 2010; published 23 Jul 2010

where $\Delta n_{eff} = n_{eff}(\omega_0) - n_{eff}(\omega_2)$. We note that Eq. (5) is an implicit non-linear equation due to the waveguide dispersion and dispersion modification due to tight bending of the waveguides. The maximum number of channels that can be packed in a WDM system using micro-rings of radii $r + \delta r_k$ with uniformly spaced channels at frequency spacing $\delta\omega$ is given by:

$$k = \frac{\Delta\omega}{\delta\omega} = \frac{1}{\delta\omega}\left(\frac{c}{r n_{eff}(\omega_2)} - \frac{\Delta n_{eff}}{n_{eff}(\omega_2)}\omega_2\right) \tag{6}$$

where floor(k) is the number of channels. For example, with an available FSR of 5000 GHz and a channel spacing of 100 GHz, 50 micro-ring modulators of 2.0 μm radius can be accommodated to provide a total bandwidth capability exceeding 500 Gbit/s.

6.3 Interconnect Bandwidth Density

The interconnect bandwidth density using WDM modulated signals with k wavelength channels with each channel modulated at bit rate B can be written as:

$$\beta = \frac{kB}{p} = \frac{kB}{0.12\log_e\left(\frac{56.6z}{\pi}\right)} \tag{7}$$

where, the pitch of the silicon waveguide array *p*, (in microns) is related to cross talk distance z (in microns) as,

$$p = 0.12\log_e\left(\frac{56.6z}{\pi}\right) \tag{8}$$

where β is the interconnect density in bits/s.μm, *p* (in microns) is the waveguide center to center pitch calculated for 250 nm X 450 nm waveguides such that a 3 dB coupling to the closest waveguide takes place for TE mode over a length of z (in microns). For example, ultra large interconnect bandwidth densities ~200 Gbit/s. μm can be achieved with 25 WDM channels operating at 12.5 Gbit/s with a 3dB coupling distance of 4 cm. One can see that a considerable design space is available using silicon micro-ring modulators to scale the modulation bandwidths & interconnect densities for future interconnect applications.

7. Conclusion

In conclusion, we show 50 Gbit/s modulation capability using silicon micro-ring carrier injection modulators. The high speed modulation capability is enabled by engineering the carrier dynamics and extending the capability using multiple wavelengths. We show large interconnect bandwidth density of 33.3 Gbit/s·μm and modulation bandwidth density > 100 Tbit/s·mm^2, both are critical figures of merit for optical networks on chip. We also discussed key design considerations for WDM systems to enable ultra large bandwidth interconnects. Scalable modulation methods based on micro-rings with novel device improvements [46–48] may meet the requirements of on-chip/chip-chip optical networks [1–8].

Acknowledgments

This work was performed in part at the Cornell NanoScale Facility, a member of the National Nanotechnology Infrastructure Network, which is supported by the National Science Foundation (Grant ECS-0335765). This work was partly supported by the Air Force Office of Scientific Research with Grant FA9550-07-1-0200 under the supervision of Dr. Gernot Pomrenke, and by the National Science Foundation (NSF) under Career Grant No. 0446571. We thank Dr. Mohammad Soltani for the comments and reviews.

#129915 - $15.00 USD Received 11 Jun 2010; revised 13 Jul 2010; accepted 13 Jul 2010; published 23 Jul 2010